Side-dependent effect in the response of valve endothelial cells to bidirectional shear stress

Emilie Faure, Eric Bertrand, Amélie Gasté, Elise Plaindoux, Valérie Deplano, Stéphane Zaffran

Side-dependent effect in the response of valve endothelial cells to bidirectional shear stress

Emilie Faure[1], Eric Bertrand[2], Amélie Gasté[1], Elise Plaindoux[1], Valérie Deplano[2,], Stéphane Zaffran[1,*]*

[1] Aix Marseille Univ, INSERM, Marseille Medical Genetics, U1251, 13005 Marseille, France

[2] Aix Marseille Univ, CNRS, IRPHE, UMR7342, 13013 Marseille, France

* Corresponding authors- Stéphane Zaffran, PhD, Marseille Medical Genetics, Aix Marseille Université, Inserm U1251, Faculté de médecine, 27 Bd Jean Moulin, 13005 Marseille, France ; stephane.zaffran@univ-amu.fr ; and Valérie Deplano, PhD, IRPHE, Aix Marseille Université, CNRS UMR7342, Technopôle de Château Gombert, 49 rue Frédéric Joliot Curie, BP146, 13384 Marseille cedex, France ; valerie.deplano@univ-amu.fr

Running title- side-specific valve endothelial cell response

Keywords- hemodynamic; aortic valve; valvular endothelial cells; wall shear stress

Abstract

Endothelial cells covering the aortic and ventricular sides of the aortic valve leaflets are exposed to different stresses, in particular wall shear stress (WSS). Biomechanical stimuli actively regulate valve tissue structure and induce remodeling events leading to valve dysfunction. Endothelial to mesenchymal transformation (EndMT), for example, has been associated with aortic valve disease. The biomechanical response of cells at different sides of the leaflets has not been clearly characterized. To analyze the mechanical response of valve endothelial cells (VECs) we developed a unique fluid activation device that applies physiologically relevant pulsatile WSS. We characterized the morphology and function of adult porcine aortic VECs derived from the opposite sides of aortic valve leaflets following exposure to different pulsatile WSS. We found that elongation and orientation of cells in response to pulsatile WSS depends on their side of origin. Quantification of gene expression confirms phenotypic differences between aortic and ventricular VECs. Aortic VECs exposed to pulsatile WSS similar to that in vivo at the tip of aortic side of the valve leaflet upregulated pro-EndMT (*ACTA2*, *Snail*, *TGFβ1*) and inflammation (*ICAM-1*, *VCAM-1*) genes, whereas expression of endothelial markers like *PECAM*-1 was decreased. Conversely, ventricular-VECs showed strong increase of *PECAM-1* expression and no activation of pro-EndMT marker. Finally, we found that stress-induced genes are upregulated in both cell types, at higher levels in ventricular compared to aortic VECs. Application of physiological shear stress levels using a fluid activation device therefore reveals functional differences in VECs derived from opposite sides of the aortic valve leaflets.

Introduction

The aortic valve maintains unidirectional blood flow between the left ventricle and the ascending aorta. Aortic valve leaflets are composed of three highly organized layers of extracellular matrix (ECM) populated by valve interstitial cells and covered by a monolayer of valve endothelial cells (VECs). The distinct layers of ECM within the leaflet are mainly composed of collagen fibers at the aortic side (*fibrosa*), elastin at the ventricular side (*ventricularis*) and proteoglycan and glycosaminoglycan (*spongiosa*) in between [1]. The composition of ECM components contributes to the structural and mechanical proprieties of the valve. Collagen provides tensile strength to the valve leaflet during opening and transfer the load to the aortic wall when the valve is closed [2]. Elastin facilitates the fast opening of the valve leaflet. The spongiosa absorbs shocks during cardiac cycle and also facilitates the relative internal rearrangements to protect the valve leaflet from damage [3]. VECs surrounding the valve leaflets are critical for circulatory function and blood-tissue interaction and can respond to changing stimuli by altering their normal functions [4]. Experimental studies have reported that aortic valve leaflets experience a wide range of wall shear stress (WSS) depending on the side (aortic or ventricular) and region (the base, belly and tip regions) at which they are located [5]. The three sub-regions of the aortic valve leaflet have been anatomically characterized by Cao and Sucosky (2017) as a region aligned along the circumferential direction, and spanning on third of the total length of the leaflet (Figure S1). While the ventricular side experiences a strong pulsatile unidirectional WSS, the aortic side experience a much lower recirculating WSS. Therefore, a WSS is a mechanical stimulus that greatly differs on either sides of the valve leaflets, and plays an important role in the development of side-dependent valve disease [6, 7]. Indeed, abnormal blood velocity and pressure can apply environmental changes, which will have consequences at the macro- to microscales promoting maladaptive tissue remodeling. Such mechanical stimuli can activate VECs, which transduce this mechanical signal to a

biochemical signal that leads to changes in gene expression and/or protein secretion, particularly of ECM components in the valve [8, 9].

At the macroscale, hemodynamic forces induce WSS on the side of the valve leaflets as well as deformation of the valve tissue under cyclic stretch. WSS modulates the function of valve cells and impacts the physiology and pathologies of these cells [10]. Recent 3D fluid structure interaction valve numerical modeling has investigated the macroscopic scale temporal and regional WSS characteristics on aortic valve leaflets under physiological flow [11, 12]. These studies confirmed side-specific differences in WSS pulsatility and magnitude between the base, belly and tip regions of the leaflets. High WSS, essentially unidirectional and pulsatile, with values comprised between 46 and 70 dyne/cm^2 near the base and the belly and reaching 93 dyne/cm^2 at the tip of the leaflet were found on the ventricular side, but were one order of magnitude lower and bidirectional on the aortic side.

Identifying how VECs respond to mechanical forces is critical to better understand aortic valve disease. The side-specificity of valve disease such as calcification might be attributed to the inherent differences in the VECs lining the aortic and ventricular sides of valve leaflets [13]. Interestingly, ~10% of VECs in human valve have been shown to undergo endothelial to mesenchymal transformation (EndMT) during development decreasing to ~1% in adult valves, suggesting heterogeneity in the phenotype of these cells [14]. To further investigate side-dependent differences in VECs we designed and used an original fluid activation device to apply controlled *in vivo* like WSS on the surface of the cells. The flow profile within the bioreactor was characterized both computationally and experimentally. Exposure of different pulsatile shear stress magnitudes to VECs confirmed a side-dependent effect. Porcine aortic VECs isolated from the two sides of the leaflets elongated and aligned differently according to the pulsatile WSS applied. Moreover, we observed a side-dependent gene expression pattern that reflected a differential response of these cells to biomechanical forces. Our results showed

that aortic-VECs undergo EndMT associated with a decrease of endothelial gene expression and an increase of inflammation genes, whereas expression of *PECAM-1* was highly increased in ventricular-VECs. Therefore, by using an original fluid activation device we highlight the side-specific phenotype of VECs lining on the two sides of the aortic valve leaflets. These data help to better understand how heterogeneity of VECs contributes to their function on different sides of the aortic valve leaflets under physiological and pathophysiological conditions.

Materials and Methods

Bioreactor design, development and functioning

A schema of the bioreactor composed of an original homemade fluid activation device linked to a specific 2D flow chamber is shown in Figure 1. An upstream glass reservoir bottle with screw cap pressure compensation (0.2 and 0.45µm filters) contains the culture medium (Figure 1A). Its volume depends on the duration to which the valve cells are submitted to WSS. Two stainless steel syringes (kdScientific) of 4.85mm inside diameter and 168.7mm overall barrel length were used (Figure 1B). One of the two syringes, filled with medium before the beginning of the experiment, injects medium in the 2D flow chamber in response to a computer generated signal. This syringe is emptied, whereas the other one, mechanically enslaved to it in an opposite manner, fills up. When the medium volume contained in one syringe tends to zero, a 3- way solenoid operated pinch valve (Bio-Chem, 100PD3MP12-02S) is automatically actuated. Meanwhile the second syringe, which is full, injects the medium into the flow chamber. C-flex tubing (3.2mm OD, 1.6mm ID, St Gobain) was used for the pinch valve to avoid potential contaminations. A downstream glass reservoir bottle was connected to the flow chamber outlet to collect the medium. Special attention was paid to avoid air bubbles within the syringes, tubing, and flow chamber.

A computer-controlled trio motion coordinator was used to drive a stepper motor (HS200-2231, Danaher motion) linked to a rolled ball screw (W1001MA-3PY-C3Z2, NSK). A gear ratio system was also added to improve displacement accuracy. This set up, using preloaded rolled ball screws with 0mm of axial play and a stepper motor with a small rotor inertia (J=340 g cm^2) enabled fast accelerations and decelerations with high accuracy.

The choice of the technical specificities used to move both syringes as well as the linking system between the engine and the syringes are the major key points that allow this original fluid

activation set-up to reproduce the WSS to which the valve cells are exposed *in vivo* in a perfectly controlled manner (see below for the validation of the activation device).

This fluid activation device is actually more adapted than commercial systems to mimic the rapid changes in flow direction. It is able to master pulsatility, accelerations, decelerations and fast variations of flowrate generating pathophysiological flow waveforms. This demonstrated its superiority in comparison to previous approaches [15-17] that used 2D flow chamber, plastic syringes and a peristaltic pump that generated steady or oscillatory flows, which do not achieve hemodynamic conditions on valvular leaflets. Finally, although Mohammed et al. [18] have used an interesting piezoelectric pumping system for studying aortic endothelial cells under pulsatile flow, their system cannot drive the values of flow rate we need in our system.

In order to impose controlled WSS on a surface we needed to master the flow behavior in a flow chamber. It is now well known that a 2D parallel plate flow chamber, with specific geometrical dimensions, permits such a control.

Assuming fully developed, laminar and incompressible flow, there exists an analytical relation between the imposed flow rate Q within the chamber and the WSS induced on its walls: $Q = \frac{WSSlh^2}{6\mu}$ where l, h and μ are the width, the thickness of the flow chamber and the fluid dynamic viscosity respectively. This relation remains true when assuming unsteady flow given the value of the frequency parameter. Consequently, $Q(t) = \frac{WSS(t)lh^2}{6\mu}$ (equation 1) and the wall shear stress on endothelial cells will be $WSS(t) = \frac{6\mu}{lh^2}Q(t)$.

The designed flow chamber was composed of three parts (Figure 1A). The upper and lower covers, 10mm thick, were machined using plexiglass. In between, the flow chamber itself, l=21mm and L=90mm, was machined using a 250µm thickness Lexan 8010 film sheet; inlet and outlet diameters were of 4mm. The fourteen stainless steel screws used for assembling the three parts ensured that the flow chamber was leak-tight. Tygon™ tubing (3.2mm OD, 1.6mm

153 ID, St Gobain) and connectors in polypropylene (Ark Plas Products™) were used to associate
154 the flow chamber to the activation device components.
155 As this flow chamber is 2D, it was important to include a 3D scaffold to culture the VECs,
156 which did not change the shear stress at the flow chamber walls but allowed for a 3D cell culture
157 environment. To do so, elliptical holes, with major and minor axis dimensions of 26mm X
158 9.8mm respectively and 2mm of depth, were drilled within the lower cover of the flow chamber
159 (Figure 1A). They were then filled with a 3D collagen gel. 3D collagen gels at a concentration
160 of 1.5 mg/mL collagen type I were made by addition of Dulbecco's Modified Eagle's Medium
161 (DMEM, Thermo Fischer Scientific), 10% fetal bovine serum (FBS, Thermo Fischer
162 Scientific), 0.1M NaOH and rat tail collagen (10 mg/mL concentration, BD Biosciences). An
163 aliquot of the collagen solution was pipetted into each well and allowed to gel for at least 1hr
164 at 37°C in 5%CO_2. VECs were seeded on the surface of the 3D collagen gels. It is worth noting
165 that the 3D collagen gel is not a model of the leaflet tissue, but provides a 3D cell culture
166 environment.
167 The dynamic viscosity of the working medium fluid was measured using a rheometer
168 HaakeMars III, fluid μ=0.945e^{-3} Pa.s. The entire set up was placed in an incubator and kept at
169 37°C and 5% CO_2 during all the experiments.
170
171 **Porcine Aortic Valve Endothelial Cells Isolation and Culture**
172 Porcine aortic valve endothelial cells (VECs) were isolated from the aortic or the ventricular
173 side of the aortic valve leaflets as previously described [16]. Porcine hearts were kindly donated
174 by the "abattoir Saint-Saturnin-lès-Apt". Briefly, aortic valve leaflets were isolated and
175 incubated in collagenase type II/DMEM (Life Technologies) for 3x7 min. After incubation cells
176 were gently scraped to isolated VECs from the two sides of the leaflets. After isolation aortic
177 or ventricular VECs were seeded and cultured on flask coated with 50ul/mL rat collagen type I

178 (10 mg/mL concentration, BD Biosciences). VECs were cultured at 37°C and 5% CO_2 in
179 Endothelial Cell Growth Medium (Promocell) supplemented with manufacturer's adjuvants
180 and 5% FBS. Endothelial cell phenotype was confirmed by qPCR. Thus, the low expression
181 levels of *ACTA2* validated the lack of contamination with other cell types such as interstitial
182 cells in the culture. The cobblestone-like morphology of valvular endothelial cells was
183 confirmed at passage 3, and cells were used at passages 3 to 6 [16].
184
185 **Immunohistochemistry**
186 Cells on collagen gels were fixed in 4% buffered paraformaldehyde during 10 min at room
187 temperature. Fixed cells were washed for 15 min three times with PBS and permeabilized with
188 0.2% Triton-X 100 (Sigma) in PBS for 10 min. Cells were washed another three times with
189 PBS before a saturation with 3% BSA and 10% Fetal Bovine Serum (Life Technologies). Cells
190 were incubated overnight with Phalloidin-iFluor 488 Reagent (F-actin; abcam) and DAPI (4',6-
191 diamidino-2-phenylindole) was used at 300 nM as a counterstain to distinguish cell nuclei. Cells
192 were photographed with a confocal LSM800 (Zeiss).
193
194 **Morphology Analysis**
195 10 representative confocal images were taken on static and exposed cells on 3D collagen I gels
196 that were fixed and stained with Phalloidin-iFluor 488 Reagent. The images were analyzed
197 using Image J2 software [19]. Images from gels exposed to WSS were aligned so that the image
198 horizontal corresponded to the direction of flow. Using Morpholib plugins on Image J2
199 software, cell area and cell perimeter were analyzed. Orientation angle between the horizontal
200 (flow direction) and the majority of F-actin filaments was also determined. Based on cell area
201 (A) and cell perimeter (P), Elongation index (Elong I) and Circularity index (shape index - SI)
202 of cells (static or exposed to the flow) were determined ($SI = 4 \pi A / P^2$ and $Elong\ I = P^2 / 4$

203 π A). Cell alignment was assessed using angle orientation data. Frequency of cells upon angle
204 orientation between 0-90°C were analyzed using Matlab software. Angle 0° were used as
205 reference to cell parallel with the flow and 90° as reference to cell perpendicular with the flow.
206 Angle orientation data from static conditions or cells exposed to fibrosa WSS (base, belly and
207 tip) were represented in polar histogram obtained using Matlab software.
208
209 **Real time quantitative PCR (qPCR)**
210 Cells were first removed from the collagen gels. Cells were lysed on Trizol (Life Technologies)
211 and RNAs were extracted using RNeasy mini Kit (Qiagen). Reverse transcriptions were
212 performed by using first strand cDNA synthesis kit (Agilent) per manufacturer's instructions.
213 LightCycler 480 SYBR Green I Master mix (Roche) was used for quantitative real-time qRT-
214 PCR analysis with a LightCycler 480 (Roche) following the manufacturer's instructions.
215 Each experiment was performed with n≥3. Samples were normalized to *TBP* as an endogenous
216 housekeeping gene. mRNA expression levels for each gene were calculated using the
217 comparative cycle threshold (ΔΔCT) method. Expression levels in the static condition were set
218 to 1. Primers used are listed in Table 1.
219
220 **Statistical Analysis**
221 All experiments were performed with n≥3. Data is expressed as mean ±SEM. Statistical
222 significance was determined using Student's *t* test to compare variances. For non-parametric
223 data, the Mann-Whitney test was used to calculate significance between the medians.
224 Interactions between conditions were initially tested with ANOVA statistics
225 (http://biostatgv.sentiweb.fr/). This test was used when it was necessary to decide whether
226 several independent groups defined by the k modalities of the study factor were from the same
227 population. p value < 0.05 was considered significant for this study.

Results

During the cardiac cycle, wall shear stress (WSS) is considered as one of the most important hemodynamic parameters for valve endothelial cells (VECs). Previous transcriptional analysis of VECs isolated from aortic valve leaflets have identified side-specific differences in VECs expression suggesting heterogeneity in the VEC phenotype [13, 20]. In order to assess the side-specificity of VECs we designed and developed an original fluid activation device able to apply a physiological controlled pulsatile WSS on the surface of VECs isolated from alternate sides of the leaflets. The temporal evolution of the WSS radial component obtained by Cao et al, 2016 (Figure 2A-C) at the base, belly and tip regions of the aortic side of the leaflets have been modeled using this original fluid activation device (see Figure S1) [11].

To analyze WSS amplitudes and waveforms, it was important to determine their amplitude WSS variation (ΔWSS) as well as their maximum, minimum and mean ($\overline{\mathrm{WSS}}$) values at base, belly and tip regions (Table 2).

Table 2 shows large amplitude WSS variations, more particularly at belly and tip regions. Both positive and negative WSS values are high compared to the mean values and the radial WSS component temporal evolutions (Figure 2A-C) highlight a significant alternation between these positive and negative values. To more accurately capture this bidirectional oscillatory waveform, oscillatory shear index, $\mathrm{OSI} = \frac{1}{2}\left(1 - \frac{\left|\int_0^T \mathrm{WSS}\,dt\right|}{\int_0^T |\mathrm{WSS}|\,dt}\right)$, [21], was also calculated. |WSS| is the norm of WSS and T, the period of cardiac cycle. This index, which is a hemodynamic factor related to oscillation flow, can vary from 0 to 0.5. When considering a WSS component, OSI will be equal to 0 if WSS is consistent and 0.5 if highly oscillatory. In the present study, we found OSI_{base}=0.38, OSI_{belly}=0.4 and OSI_{tip}=0.45. With such a high temporal oscillation of WSS during the cardiac cycle, it is obvious that VECs are exposed to strongly oscillating WSS signals far from static and steady flow conditions. In this latter case, we can also note that it

252 would not be appropriate to subject VECs to WSS mean values that are low compared to
253 maxima or minima values encountered.

254 **Validation of the flow device**

255 The flow rates were generated by controlling the displacements of the syringes, (D_s), using a
256 computer. A direct relation exists between D_s and the fluid volume, ϑ_f, injected, by the syringe:
257 $\vartheta_f = S_{sy} D_s$.with S_{sy} being the syringe section. Considering t_i the time of fluid injection Q(t) is
258 derived by $Q(t) = \frac{\vartheta_f}{t_i} = \frac{S_{sy} D_s}{t_i}$ (equation 2).

259 To validate our original fluid activation device, it was therefore important to record the syringe-
260 imposed displacements to assess their spatio-temporal accuracy. Three different WSS signals
261 computed at base, belly and tip of the aortic side were extracted from results reported in Cao et
262 al., 2016 (Figure 2A-C). Flow rates corresponding to these signals were then determined using
263 equation (1) and associated displacements of the syringe calculated using equation (2). Figure
264 2 shows the comparison between syringe-imposed displacements to generate radial WSS
265 signals related to the belly, base and tip of the aortic side and the measured ones using Solartron
266 Metrology displacement sensors (Figure 2G-I). The results highlight that the fluid activation
267 device is able to precisely reproduce the complex and fast displacement changes, which, in turn,
268 induce the WSS changes occurring during the cardiac cycle.

269 **Response of endothelial cells to mechanical environment**

270 We investigated the orientation and shape of aortic and ventricular VECs (aortic-VECs and
271 vent-VECs) following static culture or 1hr exposure to different pulsatile WSS as predicted in
272 the belly, base and tip regions of the aortic side [11]. Under static conditions, we found no
273 difference between aortic- and vent-VECs since the two cell types were randomly oriented
274 (Figure 3). Following exposure to pulsatile WSS predicted in the tip region of aortic side of the
275 leaflets, aortic-VECs did not display clear orientation. Cells were randomly oriented, as more

276 than 60% had the angle of orientation ranged from 30° and 60° (Figure 3A,B). Elongation and
277 shape index showed that aortic-VECs were mainly rounded (Figure S2). However, ventricular-
278 VECs exposed to a similar pulsatile WSS adopted an azimuthal orientation (Figure 3C, D). We
279 found that 60% of vent-VECs were orientated with the angle of orientation ranged from 45°
280 and 90°. Cell shape index analysis revealed that at equal magnitude of pulsatile WSS, vent-
281 VECs have a more elongated shape than aortic-VECs (Figure S2). Together these results show
282 that VECs isolated from the opposite sides of aortic valve leaflets have different phenotypes.

283 **Side-dependent differential gene expression**

284 To further investigate the phenotype of the two cell types we analyzed the expression of
285 different markers after an exposure of 1hr to different pulsatile WSS (related to the belly, base
286 and tip regions of the aortic side). For the aortic-VECs we quantified changes in pro-EndMT
287 (*ACTA2*, *Snail*, *TGFβ1*) genes following exposure to pulsatile WSS (Figure 4A). Compared to
288 static control, exposure to pulsatile WSS predicted in the tip region at the aortic side
289 significantly upregulated pro-EndMT gene expression (*ACTA2* 4.3±0.3 fold increase over static
290 control, $p<0.05$). Interestingly, the upregulation of *ACTA2* expression was proportional to the
291 magnitude of the pulsatile WSS applied (Figure 4B). However, ventricular-VECs exposed to
292 similar pulsatile WSS did not show comparable activation of *ACTA2* compared to aortic-VECs
293 (Figure 4B). Similarly, we did not observe significant fold change for other pro-EndMT
294 markers (Figure S3). We further analyzed the expression of the endothelial gene *PECAM-1* in
295 the two cell types. Expression of *PECAM-1* was increased in aortic-VECs exposed to pulsatile
296 WSS predicted in the base region of the aortic side of the leaflets (3.2±0.7 fold increase over
297 static control, $p<0.05$), whereas it was downregulated in cells exposed to pulsatile WSS
298 predicted in the belly and tip regions (Figure 5A). Conversely, *PECAM-1* expression was
299 strongly upregulated in ventricular-VECs after exposure to the three pulsatile WSS applied
300 (Figure 5B). For instance, expression of *PECAM-1* was highly increased in vent-VECs exposed

to pulsatile WSS predicted in the tip region (60±10 fold increase over static control, $p<0.05$). As activation of inflammatory mediators is induced by abnormal shear stress [22], we analyzed the expression of 2 inflammatory markers, *VCAM-1* and *ICAM-1*. Expression of these genes was upregulated in both cell types with some differences (Figure 6). Expression of *VCAM-1* and *ICAM-1* was increased in aortic-VECs, with the highest activation observed in cells exposed to pulsatile WSS with the greatest differential (Figure 6A; 49.5±3.7 fold increase after exposure as predicted in tip region over static control, $p<0.05$). ~~Upregulation of *NFκB* expression in aortic-VECs confirmed the activation of inflammation in this cell type with (Figure S4).~~ Although expression of *VCAM-1* and *ICAM-1* were both increased in vent-VECs (Figure 6), activation of *VCAM-1* was significantly greater in this cell type compared to its upregulation in aortic-VECs (Figure 6B; 265±17 fold increase after exposure as predicted in tip region over static control, $p<0.05$). Thus, these results suggest that the pulsatile fibrosa WSS activates expression of inflammatory markers in the vent-VECs. To analyze the activation of stress-related genes in both cell types we quantified expression of *NRF-2* and *EGR-1*, which are known to respond to shear stress in endothelial cells [23, 24]. Expression of *NRF-2* and *EGR-1* was upregulated in the two cell types, but was greater in vent-VECs compared to aortic-VECs (Figure 7A,B). Together these findings indicate that aortic- and vent-VECs behave differently to pulsatile WSS predicted in the different regions of the aortic side of aortic valve leaflets.

320 **Discussion**

321 Although the aortic valve is covered by a monolayer of endothelial cells on its two sides (aortic
322 and ventricular) the response of valve endothelial cells (VECs) to shear stress remains poorly
323 understood. Here we used a fluid activation device to show that VECs respond differently to
324 similar WSS depending on their side of origin. Shear stress is known to play a leading role in
325 endothelial cell migration and vessel remodeling. Shear stress has also been shown to result in
326 directed migration of endothelial cells against the direction of flow [25]. Our findings showed
327 differences in the alignment of aortic- vs vent-VECs to the direction of the flow. We found that
328 the orientation angle of 60% of vent-VECs was ranged between 45° to 90° when the magnitude
329 of the pulsatile WSS was highest (corresponding to WSS at the tip of the leaflet). Conversely,
330 at a similar pulsatile WSS magnitude less aortic-VECs were oriented with this angle suggesting
331 these two cell types align differently in response to flow. The alignment behaviors that we
332 observed in these two cell types may thus reflect a specific response to high WSS. The exact
333 mechanism by which VECs sense shear stress remains unclear. Several endothelial cell flow
334 sensors have been proposed for endothelial cells including integrin complexes, ion channels,
335 caveolae and complex including PECAM-1, VE-cadherin and VEGFR2 [26]. Our observations
336 suggest that the expression of *PECAM-1* was highly upregulated in vent-VECs compared to
337 aortic-VECs confirming that cell-cell contacts may be implicated in flow sensing [27]. Our data
338 are consistent with previous study that suggests distinct phenotype between VECs and vascular
339 endothelial cells in their response to blood flow [16]. Analysis at the transcriptional and protein
340 level has confirmed a transcriptional difference between VECs and aortic endothelial cells [10].
341 These data suggest that valvular endothelium acts as a distinct organ system, which may explain
342 the difference find between valvular and vascular pathology.

343 Several studies have also shown EndMT on the aortic side of adult valves, which is exposed to
344 bidirectional shear stress and is often the site of inflammatory and calcific degeneration [28,

345 29]. On the contrary, EndMT is absent at the ventricular side of the valve [30]. At this side, the
346 VECs are exposed to high unidirectional shear stress. Consistent with these observations, our
347 data show that bidirectional WSS signal induces EndMT in aortic-VECs but not ventricular-
348 VECs.

349 We showed that inflammatory markers (*VCAM-1* and *ICAM-1*) are upregulated in both
350 populations of VECs in response to physiological bidirectional WSS. The difference of *VCAM-*
351 *1* upregulation between the aortic- versus vent-VECs is consistent with a previous study
352 showing differential expression of VCAM-1 on opposite sides of normal aortic valves [13]. The
353 upregulation of *VCAM-1* and *ICAM-1* has already been demonstrated in response to TNF-α,
354 suggested a role for the hemodynamic environment in valve inflammatory process [31].
355 However, our results differ from a previous study, which demonstrated that exposure of the
356 aortic, but not ventricular, surface of the aortic valve leaflet to bidirectional shear stress
357 increases expression of inflammatory markers [22]. The WSS signal used in this previous study,
358 although bidirectional, was not physiological. More particularly the accelerating and
359 decelerating slopes as well as the frequency of flow direction changes were lower than those
360 physiologically observed. Another difference is that we used isolated VECs and not a leaflet.
361 Therefore, cells within the endothelium in intact leaflets, may be less sensitive to shear stress
362 than isolated cells. Indeed, it is known that the trilaminar structure of the leaflet protects the
363 valve, and so the VECs, from its environment (hemodynamic and biomechanics). Although
364 VECs were cultured directly on the collagen gel we observed that exposure to particular
365 conditions induced EndMT and probably invasion in the matrix, even though the collagen gel
366 has different stiffness than the ECM forming the leaflet tissue. Assessment of the effect of the
367 difference in stiffness has demonstrated that the phenotype of VECs responds to changes of the
368 3 D culture environments [32, 33]. Thus, it would be important to work on a 3D cell culture
369 environment that reproduces the physiological condition.

370 Our results confirm a previous study showing that VECs on aortic and ventricular surfaces have
371 differential gene expression profiles and, therefore, distinct phenotypes [13]. The observation
372 of morphological and functional differences between VECs isolated from the two sides of aortic
373 valve leaflets exposed to identical conditions suggests that the side-specific phenotypic
374 differences are in part intrinsic. Recent transcriptomic analysis of postnatal heart valves at
375 single cell resolution demonstrated that the endothelial cell population is separated into three
376 distinct subpopulations that display specific spatial locations in the valve leaflets [20]. The
377 VECs subset, which is characterized by classic endothelial markers, can be found on both sides
378 of porcine aortic valve leaflets. However, a particular subset of VECs is present in regions of
379 high mechanical stress, where valve leaflets are exposed to high shear [20]. Interestingly, a
380 recent study demonstrated restricted expression of Wnt9b in endothelial layer of zebrafish heart
381 valves in response to fluid forces [34]. Altogether these findings suggest a contribution of
382 biomechanical forces to maintain VEC diversity in different region of the valves.
383
384 **Conclusions**
385 In the current study, we designed and developed a unique fluid activation device that applies
386 physiologically relevant pulsatile WSS (related to the belly, base and tip regions of the leaflet).
387 We identified a clear phenotypic difference between VECs isolated from the opposite sides of
388 aortic valve leaflets. Our model replicates the physiological radial component of WSS predicted
389 in different regions of the aortic side of the aortic valve leaflet. We observed that aortic-VECs
390 undergo EndMT when bidirectional WSS, characterized by high OSI value, is applied, whereas
391 vent-VECs are less sensitive to this WSS feature. We found that VECs isolated from the two
392 sides of aortic valve leaflets induced inflammatory process, which probably respond to the
393 activation of a stress program. Our findings provide an improved understanding of phenotypic

394 differences between VEC populations in their environment and suggest that vent-VECs are less

395 subject to valve disease.

396

Acknowledgments

We thank Dr. Gaëlle Odelin for her help in collecting pig hearts. We are grateful to Dr. Robert Kelly for critically reading our manuscript. This work was supported by the "Association Française contre les Myopathies" (TRIM-RD Project), and the "Institut National de la Santé et de la Recherche Médicale" to S.Z. E.F received a postdoctoral fellowship from the "Association Française contre les Myopathies" and the "Fondation Lefoulon Delalande".

Author Contributions: conceptualization, E.F., V.D. and S.Z.; validation, E.F. and E.B.; formal analysis, E.F., E.P., A.G.; investigation, S.Z.; writing—original draft preparation, V.D. and S.Z.; writing—review and editing, V.D. and S.Z.; supervision, S.Z.; funding acquisition, S.Z.

Conflicts of Interest: The authors declare no conflict of interest. The funders had no role in the design of the study; in the collection, analyses, or interpretation of data; in the writing of the manuscript, or in the decision to publish the results.

415 **Figure legends**

416 **Figure 1: Schematic illustration of the fluid activation device.** (A) Scheme illustration of the
417 flow chamber. (B) Scheme of the bioreactor set-up for physiological wall shear stress
418 experiments.

419

420 **Figure 2: A unique fluid device system producing a pulsatile WSS.** Comparison between
421 imposed piston displacements to generate bidirectional WSS signals related to the belly of the
422 *fibrosa* leaflet side and the measured ones using Solartron Metrology displacement sensors.
423 Note that the fluid activation device is able to reproduce the complex and fast displacement
424 changes inducing the WSS changes occurring during the cardiac cycle. (A,D,G) Radial WSS
425 signals at belly, base and tip regions of the aortic side of the aortic valve leaflets from Cao et
426 al, 2016. (B,E,H) Associated flow rates. (C,F,I) Comparison between the displacements
427 imposed to generate the flow rates associated with WSS (blue symbol) and the measured values
428 (black symbol).

429

430 **Figure 3: Valve endothelial cell alignment following exposure of wall shear stress.** (A-D)
431 Valve endothelial cell (VECs) derived from opposite sides (aortic and ventricular) of aortic
432 valve leaflets were cultured under static conditions or exposed to different pulsatile wall shear
433 stress (WSS) as predicted in the base, belly and tip regions of the aortic side of the leaflets.
434 (A,C) F-actin is shown in green; nuclei are labeled with DAPI (blue). Orientation angle of VECs
435 was determined in static condition or following exposure of different pulsatile WSS and
436 displayed as a rose plot to represent the frequency and directionality of the cells. Quantification
437 of the angle between the nucleus and flow showed that 60% of vent-VECs aligned between 45°
438 and 90° to the direction of flow. White arrow indicates the direction of the flow.

439

440 **Figure 4: Valve endothelial cell phenotype following exposure to wall shear stress.** (A)
441 EndMT-related gene expression in valve endothelial cells (VECs) derived from the aortic side
442 following exposure of pulsatile wall shear stress (WSS) related to tip region of the aortic side
443 of aortic valve leaflets. (B) *ACTA-2* expression in VECs derived from opposite sides (aortic and
444 ventricular) of aortic valve following exposure of different pulsatile WSS (as predicted in the
445 base, belly and tip regions of the aortic side). qRT-PCR experiments were performed in
446 triplicate (n= 3 for each conditions) and expressed as mean ±SEM (*p<0.05 using Mann-
447 Whitney test). Expression levels in the static condition were set to 1 and all conditions were
448 compared to this reference.
449
450 **Figure 5: *PECAM-1* expression following exposure of wall shear stress.** (A,B) *PECAM-1*
451 expression in aortic-VECs (A) and ventricular-VECs (B) following exposure of different
452 pulsatile WSS (as predicted in the base, belly and tip regions of the aortic side). All experiments
453 were performed in triplicate (n= 3 for each conditions) and expressed as mean ±SEM (*p<0.05
454 versus control (static condition) according to ANOVA followed by Mann-Whitney test).
455 Expression levels in the static condition were set to 1 and all conditions were compared to this
456 reference.
457
458 **Figure 6: Expression of inflammatory markers after exposing valve endothelial cells to**
459 **wall shear stress.** *IVAM-1* and *VCAM-1* expression in VECs derived from opposite sides
460 (aortic and ventricular) of aortic valve leaflets following exposure of different pulsatile WSS
461 (as predicted in the base, belly and tip regions of the aortic side of aortic valve leaflets). All
462 experiments were performed in triplicate (n= 3 for each conditions) and expressed as mean
463 ±SEM (*p<0.05 versus control (static condition) according to ANOVA followed by Mann-

464 Whitney test). Expression levels in the static condition were set to 1 and all conditions were
465 compared to this reference.
466
467 **Figure 7: Expression of stress-related genes after exposing valve endothelial cells to wall**
468 **shear stress. (A,B)** *NRF-2* (A) and *EGR-1* (B) expression in VECs derived from opposite sides
469 (aortic and ventricular) of aortic valve leaflets following exposure of different pulsatile WSS
470 (as predicted in the base, belly and tip regions of the aortic side of aortic valve leaflets). In
471 pulsatile WSS as predicted in the tip region the expression of *NRF-2* was 2.93±1 fold increased
472 over static control ($p<0.05$) in aortic-VECs and 6.21±0.1 fold increased over static control
473 ($p<0.05$) in vent-VECs. Similarly, in pulsatile WSS as predicted in the tip region the expression
474 of *EGR-1* was 2.86±0.37 fold increased over static control ($p<0.05$) in aortic-VECs and 71.5±3
475 fold increased over static control ($p<0.05$) in vent-VECs. All experiments were performed in
476 triplicate (n= 3 for each conditions) and expressed as mean ±SEM (*$p<0.05$ versus control
477 (static condition) according to ANOVA followed by Mann-Whitney test). Expression levels in
478 the static condition were set to 1 and all conditions were compared to this reference.
479
480

481 **Supplementary figure legends**

482 **Figure S1: Schematic representation of the aortic valve.** (A) Upper view of the aortic valve.
483 (B) Lateral view of one the aortic valve leaflets. Inset shows the base, belly and tip regions on
484 the aortic valve leaflet. This drawing was inspired by the study by Cao and Sucosky (2017).

485

486 **Figure S2: Modulation of endothelial cell morphology following exposure of wall shear**
487 **stress.** Circulatory index shows that aortic and ventricular valve endothelial cells (VECs) have
488 different morphology following exposure to pulsatile wall shear stress (WSS) as predicted in
489 the base, belly and tip regions of the aortic side of the leaflets.

490

491 **Figure S3: Valve endothelial cell phenotype following exposure to wall shear stress.** (A)
492 EndMT-related gene expression in ventricular valve endothelial cells (VECs) following
493 exposure of pulsatile wall shear stress (WSS) related to tip region of the aortic side of aortic
494 valve leaflets. qRT-PCR experiments were performed in triplicate (n= 3 for each conditions)
495 and expressed as mean ±SEM. Expression levels in the static condition were set to 1 and all
496 conditions were compared to this reference.

497

498 **References**

499

500 [1] Hinton RB, Yutzey KE. Heart valve structure and function in development and disease.
501 Annual review of physiology. 2011;73:29-46.
502 [2] Schoen FJ. Mechanisms of function and disease of natural and replacement heart valves.
503 Annual review of pathology. 2012;7:161-83.
504 [3] Duan B, Kapetanovic E, Hockaday LA, Butcher JT. Three-dimensional printed trileaflet valve
505 conduits using biological hydrogels and human valve interstitial cells. Acta biomaterialia.
506 2014;10:1836-46.
507 [4] Rabkin-Aikawa E, Mayer JE, Jr., Schoen FJ. Heart valve regeneration. Advances in
508 biochemical engineering/biotechnology. 2005;94:141-79.
509 [5] Butcher JT, Nerem RM. Valvular endothelial cells and the mechanoregulation of valvular
510 pathology. Philos Trans R Soc Lond B Biol Sci. 2007;362:1445-57.
511 [6] Arjunon S, Rathan S, Jo H, Yoganathan AP. Aortic valve: mechanical environment and
512 mechanobiology. Annals of biomedical engineering. 2013;41:1331-46.
513 [7] Holliday CJ, Ankeny RF, Jo H, Nerem RM. Discovery of shear- and side-specific mRNAs and
514 miRNAs in human aortic valvular endothelial cells. American journal of physiology Heart and
515 circulatory physiology. 2011;301:H856-67.
516 [8] Balachandran K, Sucosky P, Yoganathan AP. Hemodynamics and mechanobiology of aortic
517 valve inflammation and calcification. International journal of inflammation.
518 2011;2011:263870.
519 [9] Steed E, Boselli F, Vermot J. Hemodynamics driven cardiac valve morphogenesis.
520 Biochimica et biophysica acta. 2016;1863:1760-6.
521 [10] Butcher JT, Tressel S, Johnson T, Turner D, Sorescu G, Jo H, et al. Transcriptional profiles
522 of valvular and vascular endothelial cells reveal phenotypic differences: influence of shear
523 stress. Arteriosclerosis, thrombosis, and vascular biology. 2006;26:69-77.
524 [11] Cao K, Bukac M, Sucosky P. Three-dimensional macro-scale assessment of regional and
525 temporal wall shear stress characteristics on aortic valve leaflets. Computer methods in
526 biomechanics and biomedical engineering. 2016;19:603-13.
527 [12] Cao K, Sucosky P. Computational comparison of regional stress and deformation
528 characteristics in tricuspid and bicuspid aortic valve leaflets. International journal for
529 numerical methods in biomedical engineering. 2017;33.
530 [13] Simmons CA, Grant GR, Manduchi E, Davies PF. Spatial heterogeneity of endothelial
531 phenotypes correlates with side-specific vulnerability to calcification in normal porcine aortic
532 valves. Circulation research. 2005;96:792-9.
533 [14] Paruchuri S, Yang JH, Aikawa E, Melero-Martin JM, Khan ZA, Loukogeorgakis S, et al.
534 Human pulmonary valve progenitor cells exhibit endothelial/mesenchymal plasticity in
535 response to vascular endothelial growth factor-A and transforming growth factor-beta2.
536 Circulation research. 2006;99:861-9.
537 [15] Butcher JT, Nerem RM. Porcine aortic valve interstitial cells in three-dimensional culture:
538 comparison of phenotype with aortic smooth muscle cells. The Journal of heart valve disease.
539 2004;13:478-85; discussion 85-6.
540 [16] Butcher JT, Penrod AM, Garcia AJ, Nerem RM. Unique morphology and focal adhesion
541 development of valvular endothelial cells in static and fluid flow environments.
542 Arteriosclerosis, thrombosis, and vascular biology. 2004;24:1429-34.

543 [17] Mahler GJ, Frendl CM, Cao Q, Butcher JT. Effects of shear stress pattern and magnitude
544 on mesenchymal transformation and invasion of aortic valve endothelial cells. Biotechnology
545 and bioengineering. 2014;111:2326-37.
546 [18] Mohammed M, Thurgood P, Gilliam C, Nguyen N, Pirogova E, Peter K, et al. Studying the
547 Response of Aortic Endothelial Cells under Pulsatile Flow Using a Compact Microfluidic
548 System. Analytical chemistry. 2019;91:12077-84.
549 [19] Rueden CT, Schindelin J, Hiner MC, DeZonia BE, Walter AE, Arena ET, et al. ImageJ2:
550 ImageJ for the next generation of scientific image data. BMC bioinformatics. 2017;18:529.
551 [20] Hulin A, Hortells L, Gomez-Stallons MV, O'Donnell A, Chetal K, Adam M, et al. Maturation
552 of heart valve cell populations during postnatal remodeling. Development. 2019;146.
553 [21] Ku DN, Giddens DP, Zarins CK, Glagov S. Pulsatile flow and atherosclerosis in the human
554 carotid bifurcation. Positive correlation between plaque location and low oscillating shear
555 stress. Arteriosclerosis. 1985;5:293-302.
556 [22] Sucosky P, Balachandran K, Elhammali A, Jo H, Yoganathan AP. Altered shear stress
557 stimulates upregulation of endothelial VCAM-1 and ICAM-1 in a BMP-4- and TGF-beta1-
558 dependent pathway. Arteriosclerosis, thrombosis, and vascular biology. 2009;29:254-60.
559 [23] Havis E, Duprez D. EGR1 Transcription Factor is a Multifaceted Regulator of Matrix
560 Production in Tendons and Other Connective Tissues. International journal of molecular
561 sciences. 2020;21.
562 [24] Hosoya T, Maruyama A, Kang MI, Kawatani Y, Shibata T, Uchida K, et al. Differential
563 responses of the Nrf2-Keap1 system to laminar and oscillatory shear stresses in endothelial
564 cells. The Journal of biological chemistry. 2005;280:27244-50.
565 [25] Simmers MB, Pryor AW, Blackman BR. Arterial shear stress regulates endothelial cell-
566 directed migration, polarity, and morphology in confluent monolayers. American journal of
567 physiology Heart and circulatory physiology. 2007;293:H1937-46.
568 [26] Chatterjee S, Fisher AB. Mechanotransduction in the endothelium: role of membrane
569 proteins and reactive oxygen species in sensing, transduction, and transmission of the signal
570 with altered blood flow. Antioxidants & redox signaling. 2014;20:899-913.
571 [27] Conway DE, Breckenridge MT, Hinde E, Gratton E, Chen CS, Schwartz MA. Fluid shear
572 stress on endothelial cells modulates mechanical tension across VE-cadherin and PECAM-1.
573 Current biology : CB. 2013;23:1024-30.
574 [28] Mohler ER, 3rd. Mechanisms of aortic valve calcification. The American journal of
575 cardiology. 2004;94:1396-402, A6.
576 [29] Mohler ER, 3rd, Gannon F, Reynolds C, Zimmerman R, Keane MG, Kaplan FS. Bone
577 formation and inflammation in cardiac valves. Circulation. 2001;103:1522-8.
578 [30] Mahler GJ, Farrar EJ, Butcher JT. Inflammatory cytokines promote mesenchymal
579 transformation in embryonic and adult valve endothelial cells. Arteriosclerosis, thrombosis,
580 and vascular biology. 2013;33:121-30.
581 [31] Aikawa E, Whittaker P, Farber M, Mendelson K, Padera RF, Aikawa M, et al. Human
582 semilunar cardiac valve remodeling by activated cells from fetus to adult: implications for
583 postnatal adaptation, pathology, and tissue engineering. Circulation. 2006;113:1344-52.
584 [32] Duan B, Yin Z, Hockaday Kang L, Magin RL, Butcher JT. Active tissue stiffness modulation
585 controls valve interstitial cell phenotype and osteogenic potential in 3D culture. Acta
586 biomaterialia. 2016;36:42-54.
587 [33] Yip CY, Chen JH, Zhao R, Simmons CA. Calcification by valve interstitial cells is regulated
588 by the stiffness of the extracellular matrix. Arteriosclerosis, thrombosis, and vascular biology.
589 2009;29:936-42.

590 [34] Goddard LM, Duchemin AL, Ramalingan H, Wu B, Chen M, Bamezai S, et al. Hemodynamic
591 Forces Sculpt Developing Heart Valves through a KLF2-WNT9B Paracrine Signaling Axis.
592 Developmental cell. 2017;43:274-89 e5.
593

A

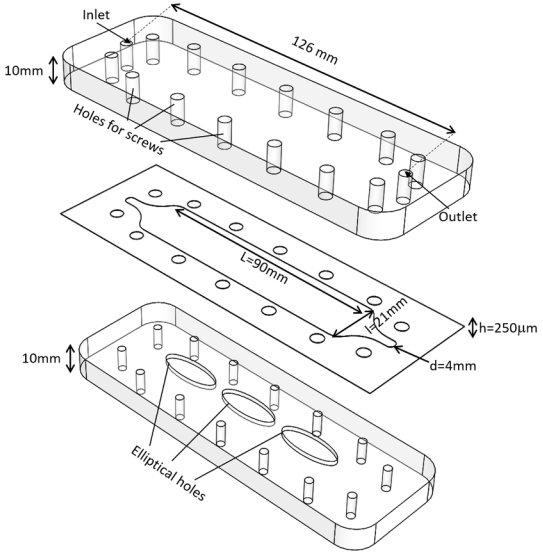
Inlet
126 mm
10mm
Holes for screws
Outlet
L=90mm
l=21mm
h=250µm
d=4mm
10mm
Elliptical holes

B

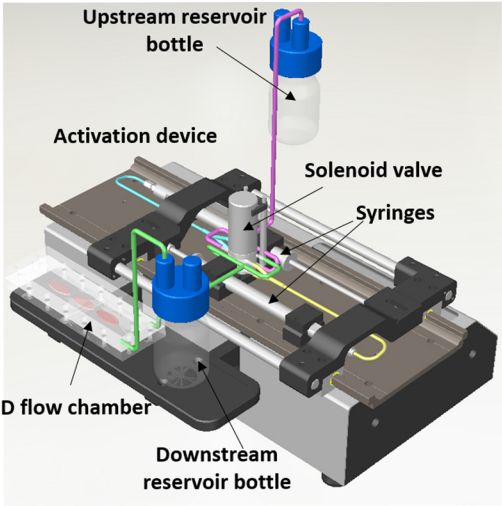
Upstream reservoir bottle
Activation device
Solenoid valve
Syringes
2D flow chamber
Downstream reservoir bottle

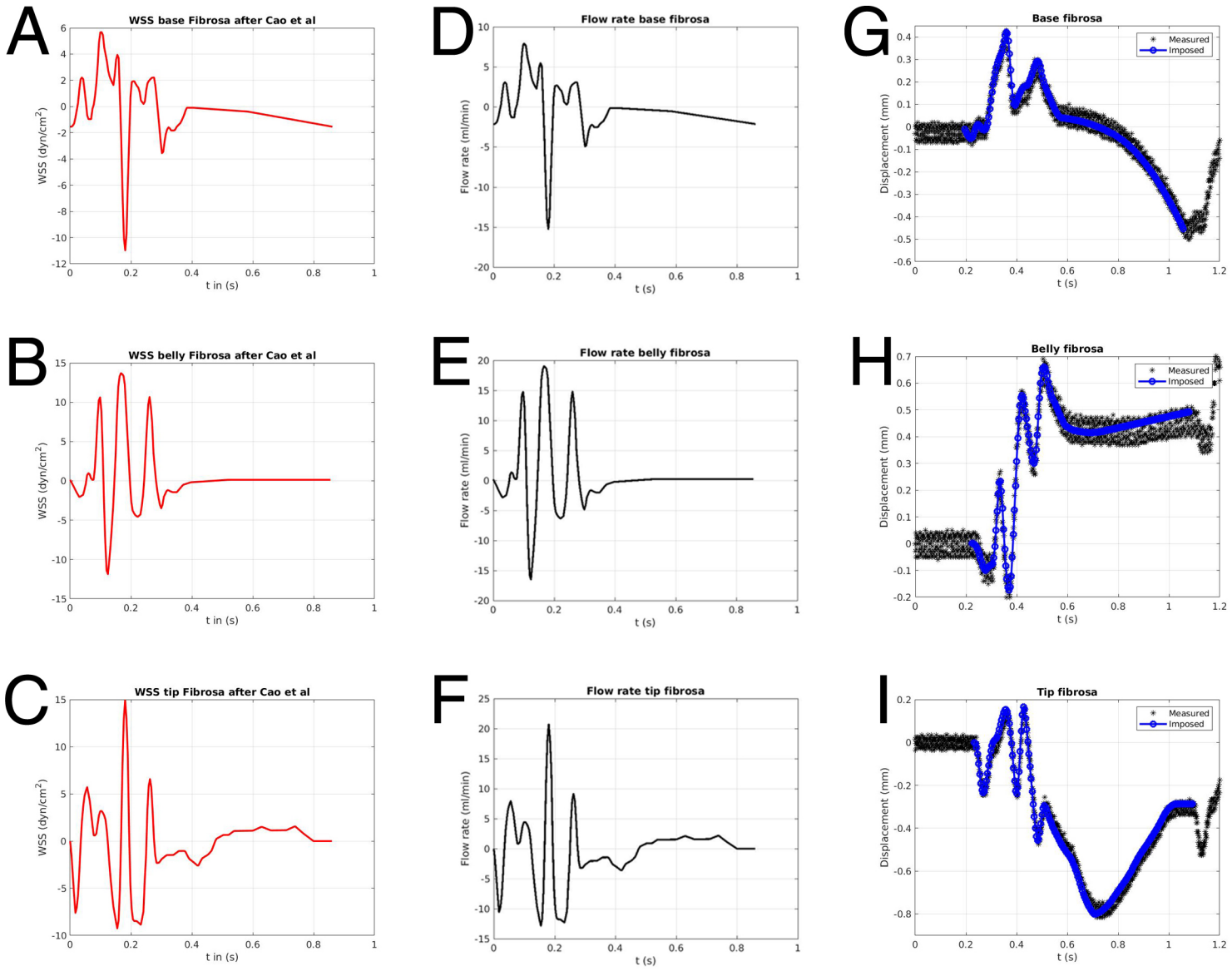
A
WSS base Fibrosa after Cao et al
WSS (dyn/cm^2)
t in (s)
B
WSS belly Fibrosa after Cao et al
WSS (dyn/cm^2)
t in (s)
C
WSS tip Fibrosa after Cao et al
WSS (dyn/cm^2)
t in (s)
D
Flow rate base fibrosa
Flow rate (ml/min)
t (s)
E
Flow rate belly fibrosa
Flow rate (ml/min)
t (s)
F
Flow rate tip fibrosa
Flow rate (ml/min)
t (s)
G
Base fibrosa
Measured
Imposed
Displacement (mm)
t (s)
H
Belly fibrosa
Measured
Imposed
Displacement (mm)
t (s)
I
Tip fibrosa
Measured
Imposed
Displacement (mm)
t (s)

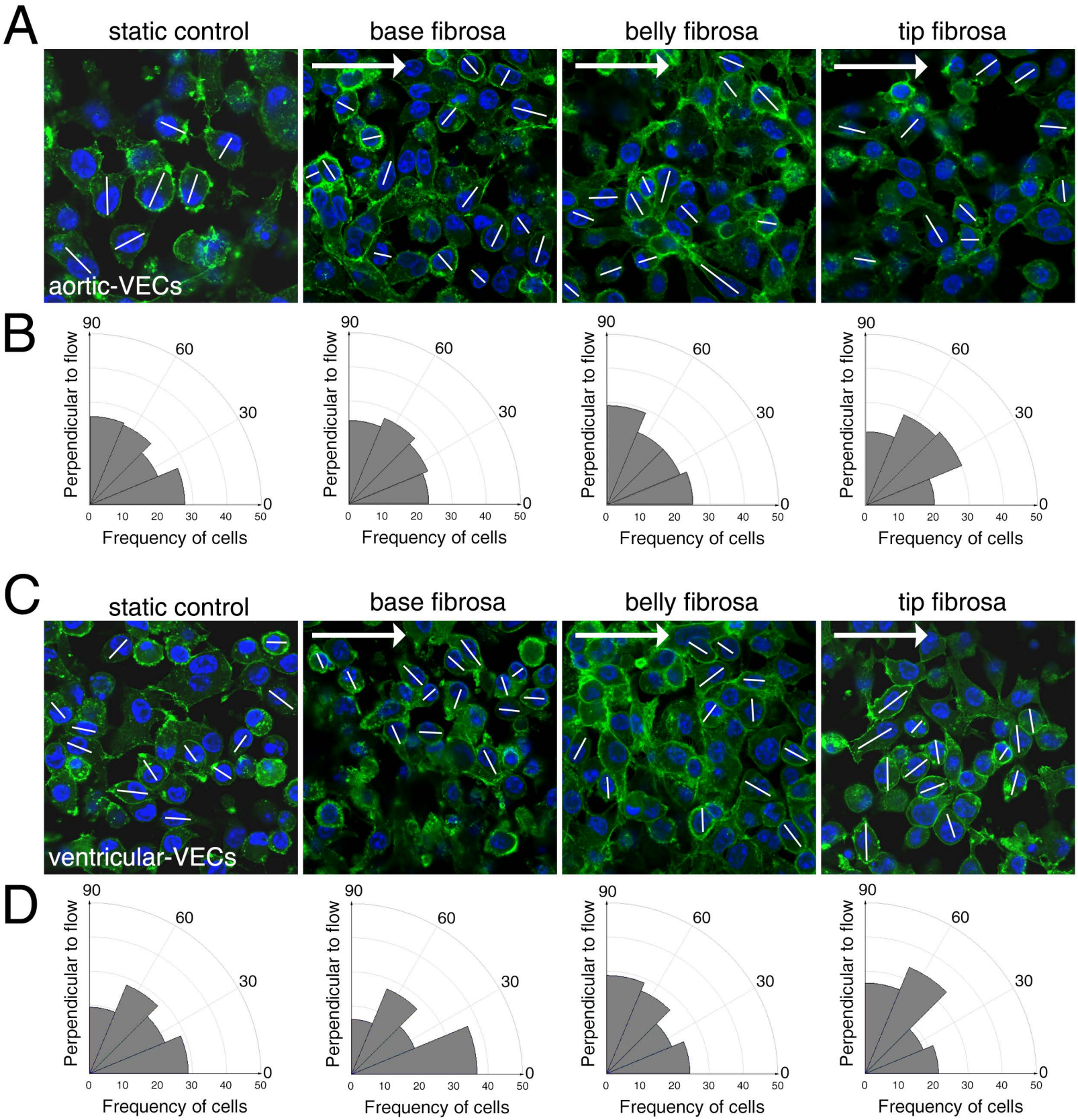
A
static control
base fibrosa
belly fibrosa
tip fibrosa
aortic-VECs
B
Perpendicular to flow
Frequency of cells
C
static control
base fibrosa
belly fibrosa
tip fibrosa
ventricular-VECs
D
Perpendicular to flow
Frequency of cells

Figure 3

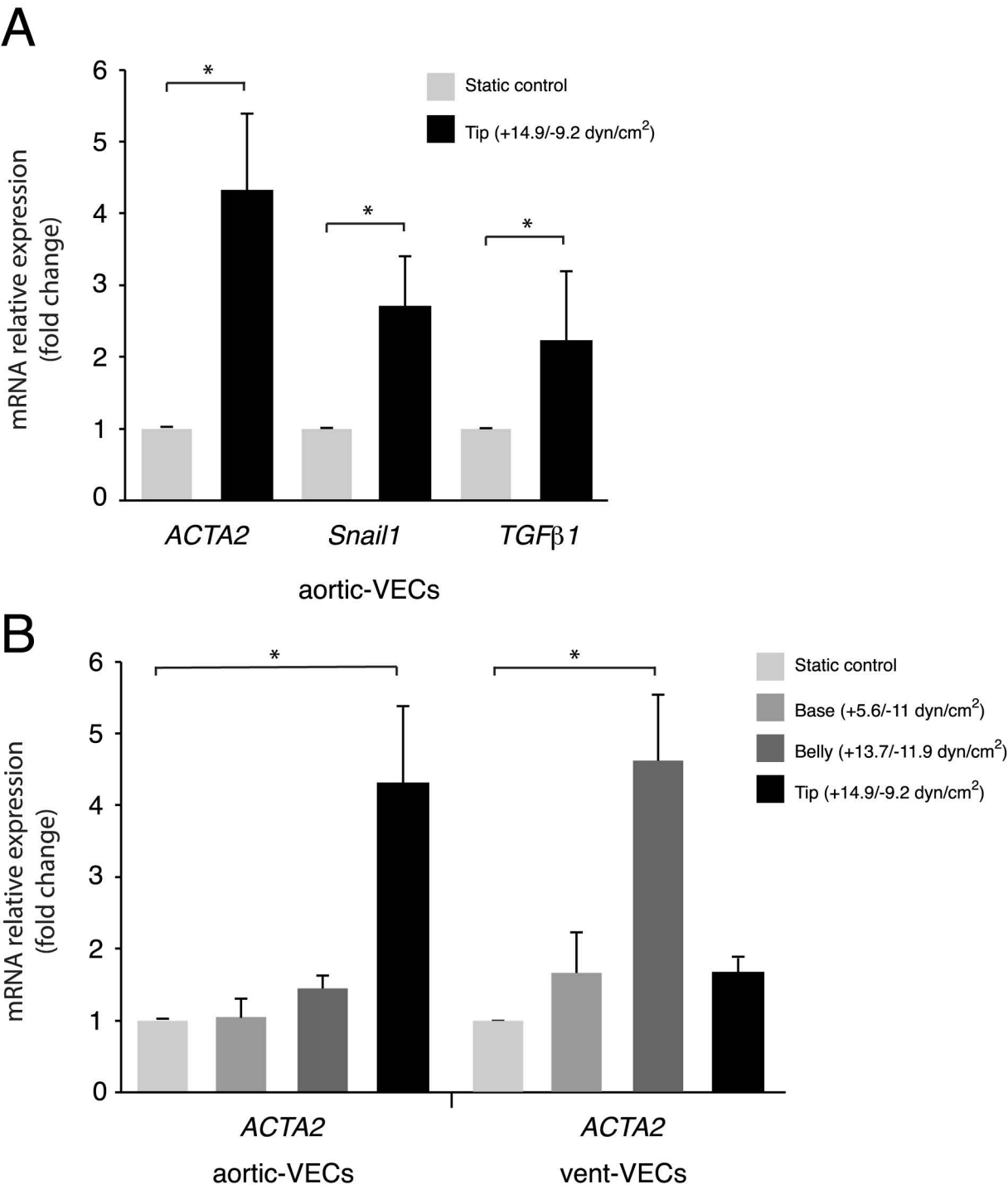
A
mRNA relative expression (fold change)
0
1
2
3
4
5
6
*
*
*
Static control
Tip (+14.9/-9.2 dyn/cm2)
ACTA2
Snail1
TGFβ1
aortic-VECs
B
mRNA relative expression (fold change)
0
1
2
3
4
5
6
*
*
Static control
Base (+5.6/-11 dyn/cm2)
Belly (+13.7/-11.9 dyn/cm2)
Tip (+14.9/-9.2 dyn/cm2)
ACTA2
aortic-VECs
ACTA2
vent-VECs

Figure 4

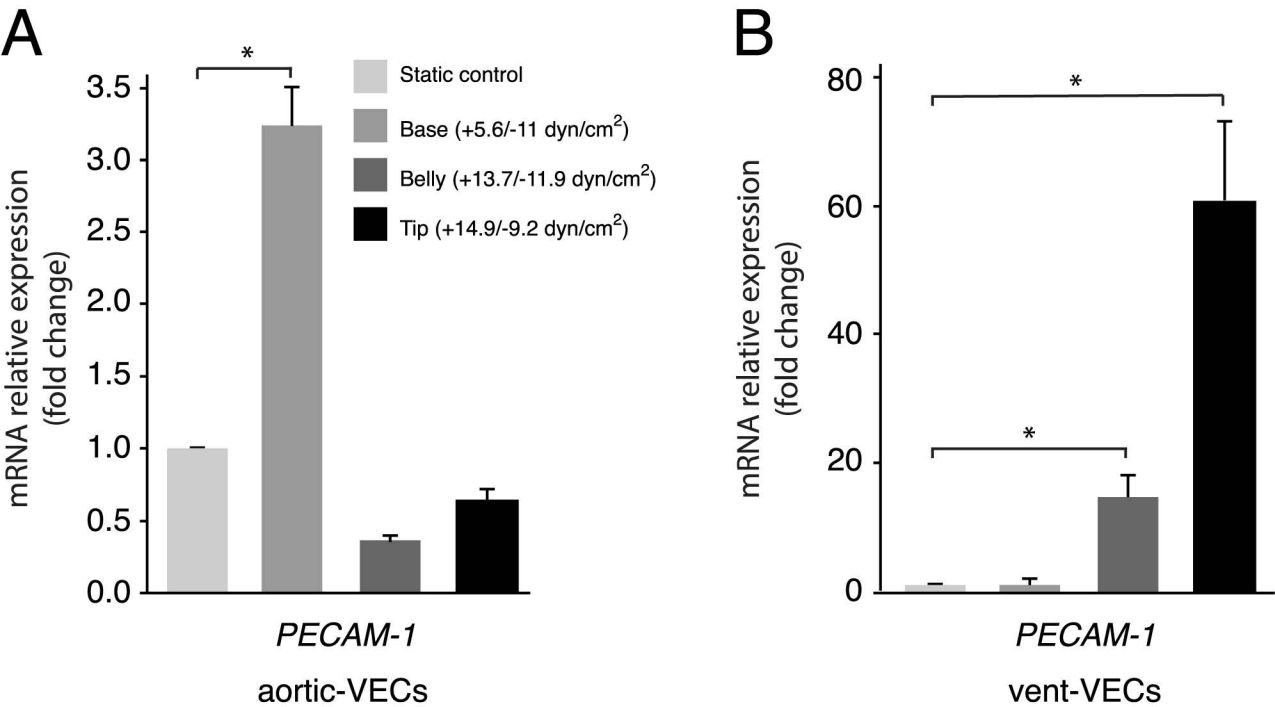
A
*
Static control
Base (+5.6/-11 dyn/cm2)
Belly (+13.7/-11.9 dyn/cm2)
Tip (+14.9/-9.2 dyn/cm2)
mRNA relative expression
(fold change)
3.5
3.0
2.5
2.0
1.5
1.0
0.5
0.0
PECAM-1
aortic-VECs
B
*
*
mRNA relative expression
(fold change)
80
60
40
20
0
PECAM-1
vent-VECs

Figure 5

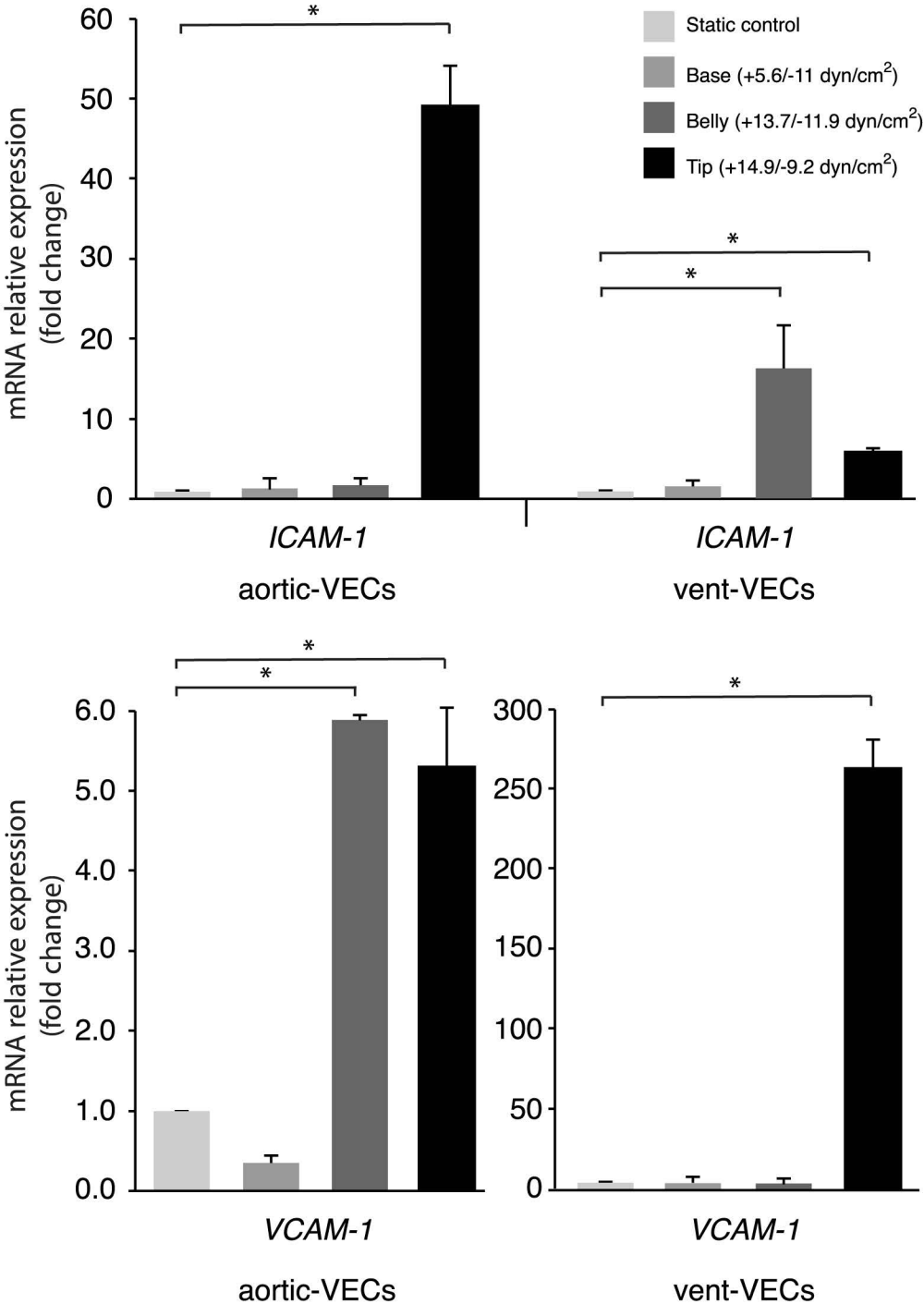
Static control
Base (+5.6/-11 dyn/cm2)
Belly (+13.7/-11.9 dyn/cm2)
Tip (+14.9/-9.2 dyn/cm2)
mRNA relative expression (fold change)
60
50
40
30
20
10
0
*
*
*
ICAM-1
aortic-VECs
ICAM-1
vent-VECs
6.0
5.0
4.0
3.0
2.0
1.0
0.0
300
250
200
150
100
50
0
VCAM-1
aortic-VECs
VCAM-1
vent-VECs

Figure 6

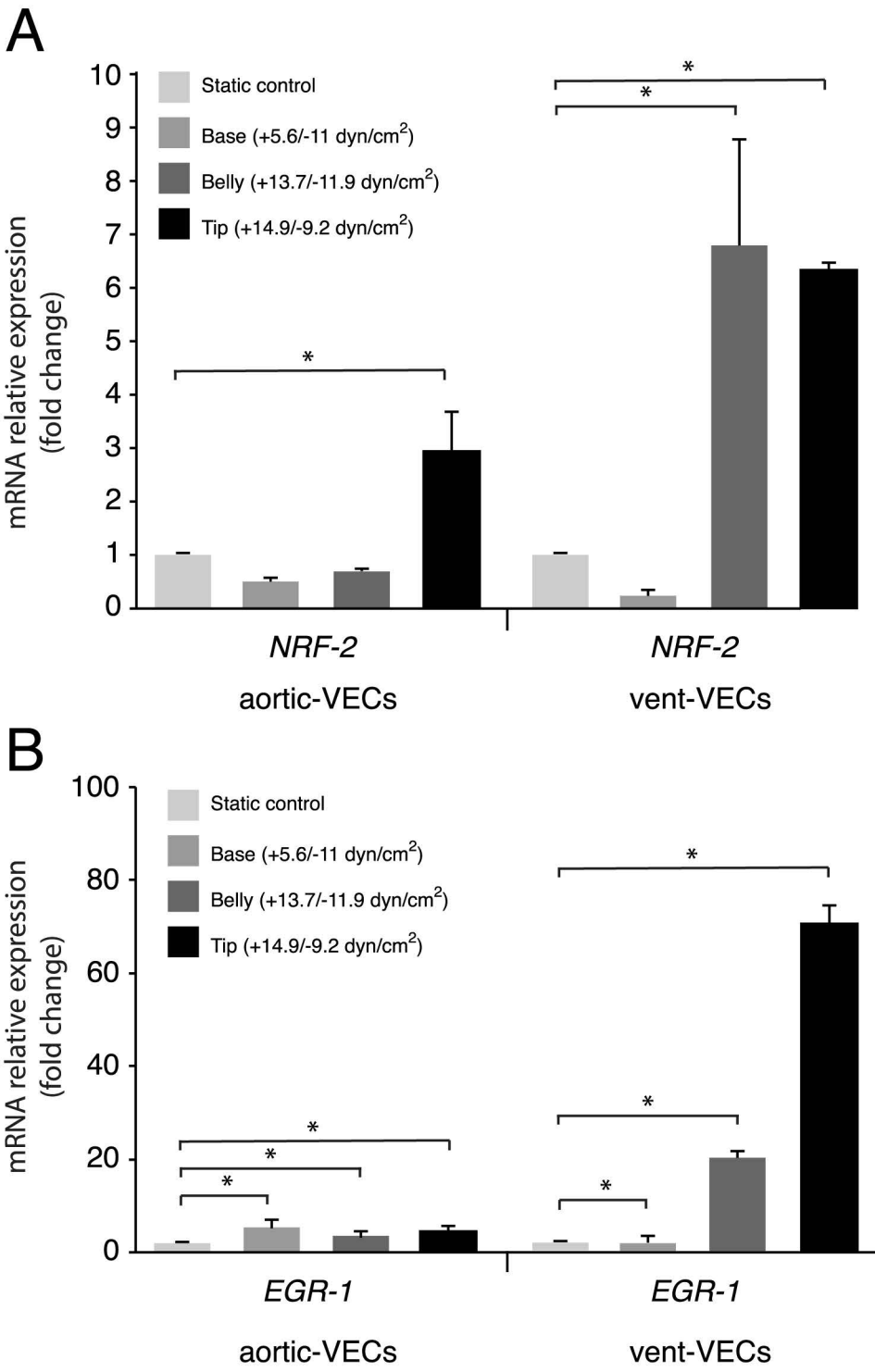
A
Static control
Base (+5.6/-11 dyn/cm2)
Belly (+13.7/-11.9 dyn/cm2)
Tip (+14.9/-9.2 dyn/cm2)
mRNA relative expression (fold change)
10
9
8
7
6
5
4
3
2
1
0
*
*
*
NRF-2
aortic-VECs
NRF-2
vent-VECs
B
Static control
Base (+5.6/-11 dyn/cm2)
Belly (+13.7/-11.9 dyn/cm2)
Tip (+14.9/-9.2 dyn/cm2)
mRNA relative expression (fold change)
100
80
60
40
20
0
*
*
*
*
*
*
EGR-1
aortic-VECs
EGR-1
vent-VECs

Figure 7